Article

Electronically Coupled MM Quadruply-Bonded Complexes (M = Mo or W) Employing Functionalized Terephthalate Bridges: Toward Molecular Rheostats and Switches

Malcolm H. Chisholm, Florian Feil, Christopher M. Hadad, and Nathan J. Patmore

J. Am. Chem. Soc., **2005**, 127 (51), 18150-18158• DOI: 10.1021/ja0550982 • Publication Date (Web): 30 November 2005

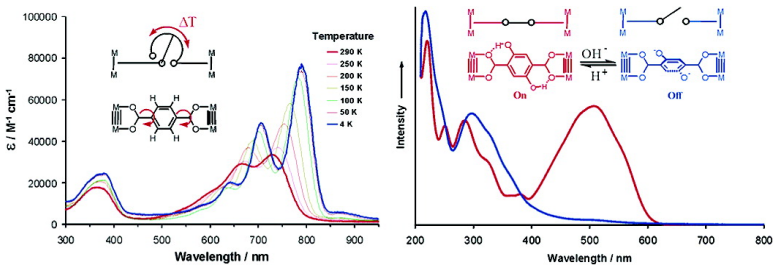

More About This Article

Additional resources and features associated with this article are available within the HTML version:

- Supporting Information
- Links to the 4 articles that cite this article, as of the time of this article download
- Access to high resolution figures
- Links to articles and content related to this article
- Copyright permission to reproduce figures and/or text from this article

View the Full Text HTML

J|A|C|S
ARTICLES
Published on Web 11/30/2005

Electronically Coupled MM Quadruply-Bonded Complexes (M = Mo or W) Employing Functionalized Terephthalate Bridges: Toward Molecular Rheostats and Switches

Malcolm H. Chisholm,* Florian Feil, Christopher M. Hadad,* and Nathan J. Patmore

Contribution from the Department of Chemistry, The Ohio State University, 100 West 18th Avenue, Columbus, Ohio 43210-1185

Received July 27, 2005; E-mail: chisholm@chemistry.ohio-state.edu; hadad.1@osu.edu

Abstract: Toluene solutions of $M_2(O_2C^tBu)_4$ (M = Mo, W; 2 equiv) react with a range of functionalized terephthalic acids, HO_2CArCO_2H (Ar = C_6H_4, C_6F_4, C_6Cl_4, C_6H_2-2,5-Cl_2, C_6H_2-2,5-$(OH)_2$, C_6H_3-2-F), to give $[(^tBuCO_2)_3M_2]_2[\mu$-$O_2CArCO_2]$. These compounds show intense ML(bridge)CT absorptions in the visible region of the electronic spectrum, and the terephthalate bridge serves to electronically couple the two M_2 units via interactions between the M_2 δ and bridge π orbitals. Electronic structure calculations reveal how the degree of electronic coupling is controlled by the dihedral angles between the terephthalate C_6 ring and the two CO_2 units and the degree of interaction between the M_4 δ MOs and the LUMO of the bridge. Both of these factors are controlled by the aryl substituents, and collectively these determine the thermochromism displayed by these complexes in solution together with the physical properties of the oxidized radical cations as determined by electrochemical studies (CV, DPV), UV−vis−NIR and EPR spectroscopic methods.

Introduction

The study of mixed-valence compounds is exemplified by the Creutz−Taube ion $[(NH_3)_5Ru(\mu$-pz$)Ru(NH_3)_5]^{5+}$, where pz = pyrazine,[1] and continues to attract considerable attention, particularly with respect to complexes that are close to the Class II/III border.[2,3] The nature of these complexes' low-energy optical spectra has recently been the subject of great interest as the profile, energy, and intensity of the IVCT absorption can yield information on the extent of electronic coupling between the metal centers.[4] MM quadruply bonded complexes, when coupled by a bridge as represented by the notation $[M_2]-X-[M_2]$, are ideally suited for studies of mixed valency for a variety of reasons. (1) The M_2 centers are redox-active and removal of an electron from an M_2 δ orbital produces a well-defined structural change in MM distance.[5] (2) When M = Mo or W, the metal atoms have several nuclei, some of which have nuclear spin [^{183}W, $I = {}^1/_2$, 15% nat. abund.; ^{95}Mo, ^{95}Mo, $I = {}^5/_2$, Σ_{abund} = 25%], thereby providing convenient spectroscopic handles. Both metals exhibit significant spin−orbit coupling, and thus EPR spectroscopy provides a uniquely powerful technique for establishing that the odd electron is associated with a metal and not a bridge and, furthermore, whether the electron is localized on one M_2 unit or delocalized over both M_2 units.[6,7] (3) The assignment of electronic transitions in the optical spectra, the $\delta \rightarrow \delta^*$ transitions, and the pronounced resonance Raman enhancement of ν(MM) are sensitive to the MM electronic configuration.[8] These three factors combine to give advantage over the now classical cases involving $L_nM(t_{2g}^5)-X-ML_n(t_{2g}^6)$.

When two MM quadruply bonded units are linked by a dicarboxylate unit $O_2C-X-CO_2$ (X = conjugated spacer), the carboxylate moieties act as alligator clips. They provide the physical points of attachment by way of covalent metal−oxygen bonds, and they provide, by way of M_2 δ-CO_2 π-conjugation, the possibility for electronic coupling of the two dinuclear units. In the case of the simplest of all dicarboxylate bridges, namely oxalate, the key orbital interactions are shown in **I** and **II** below.

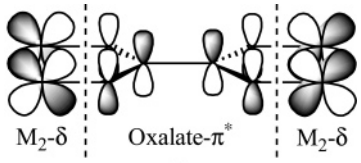

I

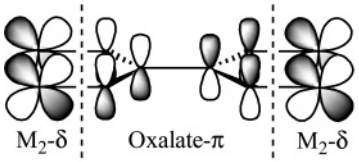

II

In **I**, the in-phase combination of M_2 δ orbitals interacts with the LUMO of the $O_2CCO_2^{2-}$ dianion. This metal-to-oxalate

(1) Creutz, C.; Taube, H. *J. Am. Chem. Soc.* **1968**, *91*, 3988.
(2) Brunschwig, B. S.; Creutz, C.; Sutin, N. *Chem. Soc. Rev.* **2002**, *31*, 168.
(3) (a) Demadis, K. D.; Hartshorn, C. M.; Meyer, T. J. *Chem. Rev.* **2001**, *101*, 2655. (b) Nelsen, S. F. *Chem.—Eur. J.* **2000**, *6*, 581. Robin, M. B.; Day, P. *Adv. Inorg. Radiochem.* **1967**, *10*, 247.
(4) Szeghalmi, A. V. et al. *J. Am. Chem. Soc.* **2004**, *126*, 7834.
(5) Cotton, F. A.; Dalal, N. S.; Liu, C. Y.; Murillo, C. A.; North, J. M.; Wang, X. *J. Am. Chem. Soc.* **2003**, *125*, 12945.
(6) Chisholm, M. H.; Pate, B. D.; Wilson, P. J.; Zaleski, J. M. *Chem. Commun.* **2002**, 1084.
(7) Chisholm, M. H.; Clark, R. J. H.; Hadad, C. M.; Patmore, N. J. *Chem. Commun.* **2004**, 80.
(8) (a) Hopkins, M. D.; Gray, H. B.; Miskowski, V. M. *Polyhedron* **1987**, *6*, 705. (b) John, K. D.; Miskowski, V. M.; Vance, M. A.; Dallinger, R. F.; Wang, L. C.; Geib, S. J.; Hopkins, M. D. *Inorg. Chem.* **1998**, *37*, 6858.

10.1021/ja0550982 CCC: $30.25

back-bonding places electron density into the $O_2CCO_2^{2-}$ π^*-orbital, which is C−C π bonding, and favors a planar oxalate bridge in contrast to the preferred staggered D_{2d} structure of the free dianion.[9] The interaction shown in **II** is a filled−filled interaction and serves to raise the energy of the out-of-phase δ combination. Based on relative orbital energies, the interaction depicted by **I** is most important and is greater for tungsten relative to molybdenum in closely related compounds.

From previous studies, we know that the energetic preference for the planar oxalate bridge is only modest and has been estimated to be ∼4−5 kcal mol^{-1} for M = Mo and 8−9 kcal mol^{-1} for M = W.[10] The larger rotational barrier for M = W reflects a greater degree of back-bonding to the bridge. The LUMO of these complexes is an oxalate π^* orbital, which has extensive mixing with the in-phase M_2 combination, **I**. Similarly for terephthalate the lowest energy, fully allowed, electronic transition involves the HOMO and LUMO orbitals and is metal-to-bridge charge transfer. The HOMO−LUMO energy gap and the electronic coupling of the two M_2 centers is governed by the two dihedral angles between the $-CO_2$ and Ar planes, θ_1 and θ_2, shown below in **III**. These dihedral angles serve as a

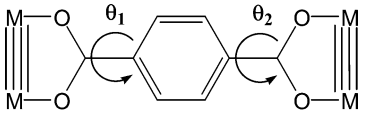

III

molecular rheostat: the planar D_{2h} structure with $\theta_1 = \theta_2 = 0°$ representing "on" and $\theta_1 = \theta_2 = 90°$ representing "off". In solution, the selection of temperature and solvent leads to thermo- and solvatochromic behavior for these bridged complexes.[11]

In this paper, we describe our syntheses and characterizations of a series of arylbridged dicarboxylates of the form [(^{t}-BuCO$_2$)$_3$M$_2$]$_2$[μ-O$_2$C−Ar−CO$_2$], where M = Mo or W. Since metal−ligand distances are essentially the same for both metals (M = Mo or W) and the M_2-to-M_2 separation is constant at ∼11 Å, this system is, in many ways, ideal with respect to examining the influence of electronic factors associated with the M_2 unit and the bridge and the way in which these factors can be employed to modulate and control the coupling of the two M_2 units. The preparation and characterization of the perfluoroterephthalate complexes were previously reported.[6,12,13]

Experimental Section

Physical Techniques. X-band EPR spectra were recorded using a Bruker ESP300 Electron Spin Resonance spectrometer. Temperature regulation was achieved by employing a Bruker Variable Temperature Unit. UV/vis/NIR spectra were recorded using a PerkinElmer Lambda 900 UV/vis/NIR spectrometer, with nitrogen purging. IR quartz cells with 1.00 or 10.00 mm path lengths were employed with sample concentrations of ∼10^{-4} and ∼10^{-5} M, respectively. The background spectrum of the neat solvent (THF) was subtracted.

^{1}H NMR spectra were recorded on a 400 MHz Bruker DPX Avance spectrometer and referenced to residual protio signals of d_8-THF at δ = 3.58 and 1.73 ppm. Cyclic voltammograms and differential pulse voltammograms were collected at scan rates of 100 mV s^{-1} and 5 mV s^{-1}, respectively, using a Princeton Applied Research (PAR) 173A potentiostat-galvanostat equipped with a PAR 176 current-to-voltage converter. Electrochemical measurements were performed under an inert atmosphere in a 0.1 M solution of ^{n}Bu$_4$NPF$_6$ in THF inside a single-compartment voltammetric cell equipped with a platinum working electrode, a platinum wire auxiliary electrode, and a pseudo-reference electrode consisting of a silver wire in 0.1 M ^{n}Bu$_4$NPF$_6$/THF separated from the bulk solution by a Vycor tip. The potentials are referenced internally to the $FeCp_2/FeCp_2^+$ couple by addition of a small amount of $FeCp_2$ to the solutions of the complexes. Microanalysis was performed by Atlantic Microlab, Inc.

Matrix assisted laser desorption/ionization time-of-flight (MALDI-TOF) was performed on a Bruker Reflex III (Bruker, Breman, Germany) mass spectrometer operated in linear, positive ion mode with a N_2 laser. Laser power was used at the threshold level required to generate signal. Accelerating voltage was set to 28 kV. Dithranol was used as the matrix and prepared as a saturated solution in THF. Allotments of matrix and sample were thoroughly mixed together; 0.5 mL of this mixture was spotted on the target plate and allowed to dry prior to laser excitation.

Electronic Structure Calculations. Electronic structure calculations on the model compounds [(HCO$_2$)$_3$M$_2$]$_2$[μ-O$_2$CArCO$_2$] (M = Mo, W; Ar = C_6H_4, C_6F_4, C_6Cl_4, $C_6H_2Cl_2$) were performed using density functional theory with the aid of the Gaussian03 suite of programs.[14] The B3LYP functional[15] along with the 6-31G*(5d) basis set[16] were used for H, C, O, F, and Cl along with the SDD energy consistent pseudopotentials for molybdenum and tungsten.[17] Geometry optimizations were performed in the appropriate symmetry, and local minima were confirmed on the potential energy surfaces using harmonic vibrational frequency analyses.

Synthetic Work. Standard glovebox and Schlenk line techniques were used to manipulate all compounds. Solvents were dried by refluxing over the appropriate drying agent and degassed prior to use. Mo$_2$(O$_2$C^{t}Bu)$_4$,[18] W$_2$(O$_2$C^{t}Bu)$_4$,[19] and [(^{t}BuCO$_2$)$_3$W$_2$]$_2$[μ-C$_6$F$_4$-1,4-(CO$_2$)$_2$][13] were synthesized according to previously published literature procedures. All other compounds were purchased from commercial sources and used without further purification. The radical cations of the cations were generated in situ prior to UV/vis/NIR and EPR spectroscopic measurements due to their instability, by treatment with 1 equiv of $AgPF_6$ in THF solutions.

Details of the preparations of the new compounds and their characterizations are given in the Supporting Information.

Results and Discussion

Syntheses. The compounds were prepared according to the metathesis reaction shown in eq 1, where the tetranuclear complexes were formed as microcrystalline products. These intensely colored, air-sensitive compounds are insoluble in toluene and benzene but are appreciably soluble in tetrahydrofuran.

(9) (a) Clark, R. J. H.; Firth, S. *Spectrochim. Acta, Part A* **2002**, *58*, 1731. (b) Dewar, M. J. S.; Zheng, Y. J. *THEOCHEM* **1990**, *68*, 157.
(10) Bursten, B. E.; Chisholm, M. H.; Clark, R. J. H.; Firth, S.; Hadad, C. M.; MacIntosh, A. M.; Wilson, P. J.; Woodward, P. M.; Zaleski, J. M. *J. Am. Chem. Soc.* **2002**, *124*, 3050.
(11) Chisholm, M. H.; Patmore, N. J. *Inorg. Chim. Acta* **2004**, *357*, 3877.
(12) Bursten, B. E.; Chisholm, M. H.; Clark, R. J. H.; Firth, S.; Hadad, C. M.; Wilson, P. J.; Woodward, P. M.; Zaleski, J. M. *J. Am. Chem. Soc.* **2002**, *124*, 12244.
(13) Cayton, R. H.; Chisholm, M. H.; Huffman, J. C.; Lobkovsky, E. B. *J. Am. Chem. Soc.* **1991**, *113*, 8709.
(14) Frisch, M. J., et al. *Gaussian 03*, Revision B.04; Gaussian, Inc.: Pittsburgh, PA, 2003.
(15) (a) Becke, A. D. *Phys. Rev. A: At., Mol., Opt. Phys.* **1988**, *38*, 3098. (b) Becke, A. D. *J. Chem. Phys.* **1993**, *98*, 5648. (c) Lee, C.; Yang, W.; Parr, R. G. *Phys. Rev. B: Condens. Matter* **1988**, *37*, 785.
(16) Hehre, W. J.; Radom, L.; Schleyer, P. v. R.; Pople, J. A. *Ab initio Molecular Orbital Theory*; John Wiley & Sons: New York, 1986.
(17) Andrae, D.; Haeussermann, U.; Dolg, M.; Stoll, H.; Preuss, H. *Theor. Chim. Acta* **1990**, *77*, 123.
(18) Brignole, A. B.; Cotton, F. A. *Inorg. Synth.* **1971**, *13*, 81.
(19) Santure, D. J.; Huffman, J. C.; Sattelberger, A. P. *Inorg. Chem.* **1985**, *24*, 371.

$$2M_2(O_2C^tBu)_4 + 1,4\text{-}Ar(CO_2H)_2 \rightarrow [(^tBuCO_2)_3M_2]_2[\mu\text{-}O_2CArCO_2] + 2\,^tBuCOOH \quad (1)$$

(Ar = C_6H_4, C_6F_4, C_6Cl_4, C_6H_2-2,5-Cl_2, C_6H_2-2,5-$(OH)_2$, C_6H_3-2-F; M = Mo, W)

The mixed valence radical cations were prepared by oxidation with $AgPF_6$ in THF. The tetranuclear radical cations are not chemically persistent and were not isolated in the solid state. Their spectroscopic properties were examined on freshly prepared solutions.

The use of 1,4 substituted phenyl rings was done to obtain maximum electronic coupling through the aryl bridge, and the selection of substituents on the arene ring was made in order to probe how the electronic coupling correlates with the O_2C-C_6 ring dihedral angles (θ_1 and θ_2) and with the HOMO−LUMO energy gap. Because the degree of coupling is notably less for M = Mo, the major focus of the work has been with tungsten complexes.

Computational Studies of Electronic Structure. Electronic structure calculations were carried out on the model compounds $[(HCO_2)_3M_2]_2[\mu\text{-}O_2CArCO_2]$ employing density functional theory and time-dependent density functional theory (DFT and TD-DFT, respectively) with the aid of the Gaussian 03 suite of programs.[14] Ground-state geometry optimizations were carried out using the B3LYP functional[15] along with the SDD energy consistent pseudopotentials for molybdenum and tungsten[17] and the 6-31G* basis set[16] for all of the other atoms (see Experimental Section).

An estimation of rotational energy barriers was determined by calculations where the CO_2-C_6 ring dihedral angles (θ_1 and θ_2) were varied independently in 10° increments, with all of the other parameters being fully optimized. The minimum energy barrier to rotation occurs where one M_2 moiety is rotated while the other dinuclear center remains at its minimum energy configuration. When Ar = C_6X_4 (X = H and F), the planar structure having D_{2h} symmetry ($\theta_1 = \theta_2 = 0°$) is the minimum energy structure as it maximizes back-bonding from the M_2 δ-to-bridge π^* orbitals. However, the calculated rotational energy barriers are $C_6H_4 > C_6F_4$ due to more significant CX···O peri interactions for C_6F_4. For Ar = C_6Cl_4, CCl···O interactions favor a twisted ground-state structure with ($\theta_1 = \theta_2 = 57°$). In this instance, there are two rotational barriers, and the one with the M_2-O_2C unit coplanar with the C_6 ring is calculated to be the higher. In the case of X = OH, the planar C_{2v} structure is the preferred ground-state conformation, and the gas-phase calculation implicates intramolecular OH···O_2C hydrogen bonding resulting in a significantly higher barrier to ring-rotation. The similarity of the calculated rotational barrier for M = Mo (11.7 kcal mol^{-1}) and M = W (12.4 kcal mol^{-1}) implies that, in this instance, hydrogen bonding dominates metal-to-ligand back-bonding in controlling the rotational barriers.

For the compounds derived from nonpolar disubstituted bridges of the form C_6H_2-2,5-Cl_2-1,4-$(CO_2H)_2$, a near planar ($\theta_1 = \theta_2 = 15°$) ground-state structure was calculated to be preferred. Again, this effect results in two rotational barriers, but this time the structure with $\theta_1 = 90°$ is the higher energy transition state geometry.

Two polar-bridged complexes were studied in this work: (1) a monofluorinated C_6H_3-2-F ring and (2) a 2,6-dichlorinated ring C_6H_2-2,6-Cl_2. The former favors a planar C_s ($\theta_1 = \theta_2 = 0°$) ground state, and the latter has one O_2C-C_6 unit planar and the other, the one with adjacent CCl groups, twisted ($\theta_1 = 0°$, $\theta_2 = 90°$).

Table 1. Summary of the Calculated Properties for $[(HCO_2)_3M_2]_2[\mu\text{-}O_2C-Ar-CO_2]$ (M = Mo, W) Compounds[a]

Ar	calculated ground-state conformations (θ_1,θ_2)[b]/deg	rotational barrier[c]/ kcal mol^{-1}	calculated HOMO–LUMO gap/eV
	M = W		
C_6H_4	0,0	9.6	2.48
C_6F_4	0,0	4.6	2.25
C_6Cl_4	57,57	1.1	2.74
$C_6H_2-2,5\text{-}Cl_2$	15,15	0.3	2.34
$C_6H_2-2,5\text{-}(OH)_2$	0,0	12.4	2.52
$C_6H_3-2\text{-}F$	0,0	5.4	2.40
$C_6H_2-2,6\text{-}Cl_2$	90,0	2.8	2.67
	M = Mo		
$C_6H_2-2,5\text{-}(OH)_2$	0,0	11.7	3.04

[a] Rotational barriers were calculated from the difference in energy between the ground-state conformation and the highest energy conformation upon rotation of one M_2 moiety with respect to the C_6-ring. [b] θ_1 and θ_2 represent the dihedral angles for each Ar ring relative to either adjacent O_2C- unit. [c] In the case of asymmetric bridges, the lowest rotational energy barrier is given.

A summary of the calculated ground state conformations, the calculated rotational barriers, and the calculated HOMO−LUMO energy gaps is given in Table 1.

Bonding Considerations. As was described earlier for the perfluoroterephthalate-bridged (Ar = C_6F_4) complexes,[12] the key orbital interactions involving the M_2 δ's and the bridge π-orbitals leads to a splitting of the M_2 δ MOs. The HOMO-1 is stabilized as a result of M_2-to-bridge back-bonding. The LUMO is bridge centered, and the HOMO−LUMO electronic transition is fully allowed and is an MLCT ($\delta \rightarrow \pi^*$) absorption based on TD-DFT calculations. The higher energy of the W_2 δ MOs leads to a decrease in the HOMO−LUMO gap and a greater splitting of the two M_2 δ combinations than that for Mo. As the dihedral angle between the CO_2 unit and the C_6 ring increases, the HOMO−LUMO energy gap increases and the splitting of the two M_2 δ MOs goes to zero when $\theta = 90°$ for both CO_2-C_6(ring) dihedrals. These frontier orbital interactions are represented in Figure 1. The LUMO is depicted in **IV** below, and has quinoidal character as depicted by the resonance structure shown.

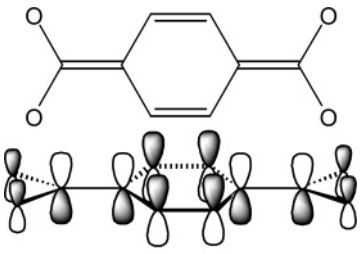

IV

In the asymmetric polar-bridged compounds, the two M_2 units are inequivalent, but for the monofluoroaryl bridged compound, the asymmetry is not calculated to be significant. In the case of the 2,6-dichloro aryl bridge, the HOMO is an M_2 δ orbital largely centered on the M_2 unit furthest away from the chloro

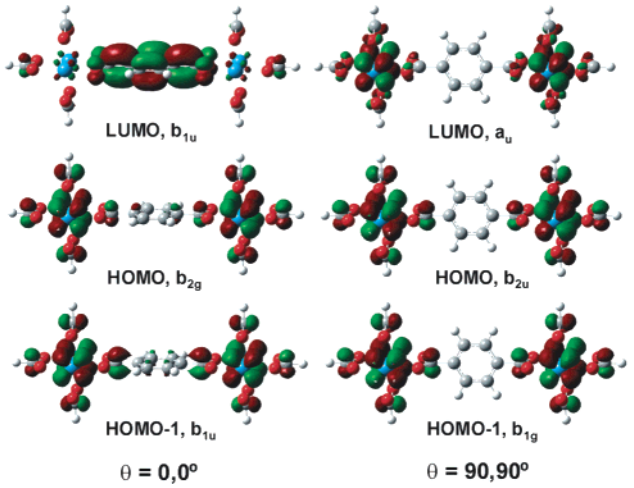

Figure 1. Frontier molecular orbital diagrams for $\theta_1 = \theta_2 = 0°$ and $\theta_1 = \theta_2 = 90°$ of $[(^t BuCO_2)_3W_2]_2[\mu\text{-}O_2C{-}C_6H_4{-}CO_2]$. Orbitals are drawn with an isosurface value of 0.02 au.

Table 2. Comparison of the Experimentally Observed MLCT ($\delta \rightarrow \pi^*$) Electronic Transition in the UV/vis Spectra of $[(^t BuCO_2)_3M_2]_2[\mu\text{-}O_2C{-}Ar{-}CO_2]$ (M = Mo, W) Compounds[a]

Ar	λ_{max}/nm	λ_{max}/eV	ϵ/M^{-1} cm^{-1}
	M = W		
C_6H_4	727	1.71	33 110
C_6F_4	825	1.50	24 800
C_6Cl_4	609	2.04	4760
$C_6H_2{-}2,5\text{-}Cl_2$	804	1.54	45 280
$C_6H_2{-}2,5\text{-}(OH)_2$	758	1.64	47 580
$C_6H_5{-}2\text{-}F$	746	1.66	28 110
$C_6H_2{-}2,6\text{-}Cl_2$	712	1.74	19 710
	M = Mo		
C_6F_4[b]	470	2.64	10 500
$C_6H_2{-}2,5\text{-}(OH)_2$	508	2.44	16 070

[a] Spectra were obtained in THF solutions (concentration ~10^{-4} M) at 298 K. [b] Values obtained from ref 13.

groups and the HOMO-1 is centered on the M_2 unit adjacent to the chlorinated and twisted aromatic group.

Electronic Absorption Spectra. The Neutral Complexes. The observed electronic transitions for the $[(^t BuCO_2)_3M_2]_2[\mu\text{-}O_2CArCO_2]$ compounds are summarized in Table 2. Apart from Ar = C_6H_2-2,5-$(OH)_2$, the intense absorptions in the visible region of the electronic spectrum roughly track with the trend seen for the calculated HOMO−LUMO energy gaps (see Table 1). The calculated energy of these transitions is always high because the calculations do not sufficiently take into account the degree of spin−orbit coupling for the heavy W atom. A nice comparison of the room temperature spectra of the W_4-containing compounds with the $O_2C{-}C_6X_4{-}CO_2$ bridges where X = H, F and Cl is given in Figure 2. Both the band shapes and the energies of this ML(bridge)CT transition are accommodated by the predictions given in Table 1. The higher energy and weaker broad transition of the tetrachloroaryl-bridged compound arises because the ground-state geometry is not planar but rather has $\theta = 57°$. This leads to poor M_2 δ-to-bridge overlap and a large HOMO−LUMO energy gap (in relation to what the planar form of the molecule would have). The spectra of the compounds where X = H and F are also particularly informative. For X = F, the absorption is much broader at 298 K, while, for X = H, one sees a relatively sharp onset of the (0,0) adiabatic transition and clear evidence of a vibronic progression. This correlates with the prediction that the rotational

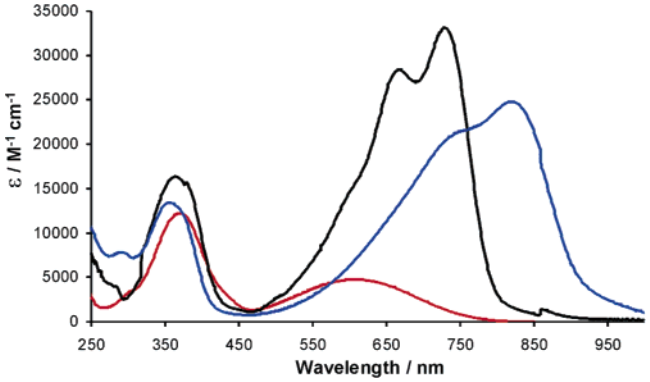

Figure 2. Electronic absorption spectra of $[(^t BuCO_2)_3W_2]_2[\mu\text{-}O_2C{-}C_6X_4{-}CO_2]$ [X = F (blue), H (black), and Cl (red)] in THF at room temperature. The spectral feature at 860 nm is due to a grating change in the spectrometer.

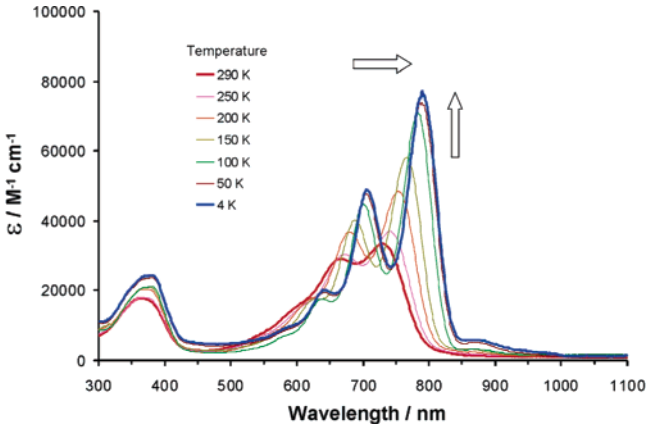

Figure 3. Electronic absorption spectra of $[(^t BuCO_2)_3W_2]_2[\mu\text{-}O_2C{-}C_6H_4{-}CO_2]$ in 2-MeTHF taken at temperatures between 290 K (red) and 4 K (blue).

barriers are of the order X = H (9.6 kcal mol^{-1}) and X = F (4.6 kcal mol^{-1}).

Upon cooling samples in 2-MeTHF, the spectra of all the compounds show some degree of a bathochromic shift, and the magnitude of this follows the order X = F > H ≫ Cl, which is consistent with the calculated rotational energy barriers. The variations with temperature for the terephthalate (X = H) are shown in Figure 3.

At the low temperature limit in the 2-MeTHF glass, the (0,0) transition is relatively sharp and very intense: for X = H, $\epsilon \approx$ 80 000 M^{-1} cm^{-1}, and for X = F, $\epsilon \approx$ 140 000 M^{-1} cm^{-1}. For X = H, the vibronic progression is very pronounced and shows evidence of anharmonicity: $\nu_1' = 1550$ cm^{-1}; $\nu_2' = 1440$ cm^{-1} and $\nu_3' = 1390$ cm^{-1}. Given the resolution of the vibronic features, these can, of course, only be claimed as estimates. Nevertheless, this vibronic progression surely correlates with ν(CC) of the bridge in accordance with placing an electron in the LUMO which is C−O π^* and C−C π bonding as shown in **III**. Just before the onset of the (0,0) transition, there is a weaker absorption to lower energy, $\epsilon \approx$ 5000 M^{-1} cm^{-1}, which we propose is the spin forbidden singlet-to-triplet transition, which gains intensity due to spin−orbit coupling with the 5d element tungsten. We note that this transition is not present in the ML(bridge)CT absorption of the radical cations, vide infra, for which a singlet to triplet transition is not possible.

At higher energies and shorter wavelength, ca. 390 nm for M = W, there are also strong absorptions, $\epsilon \approx$ 15 000 M^{-1}

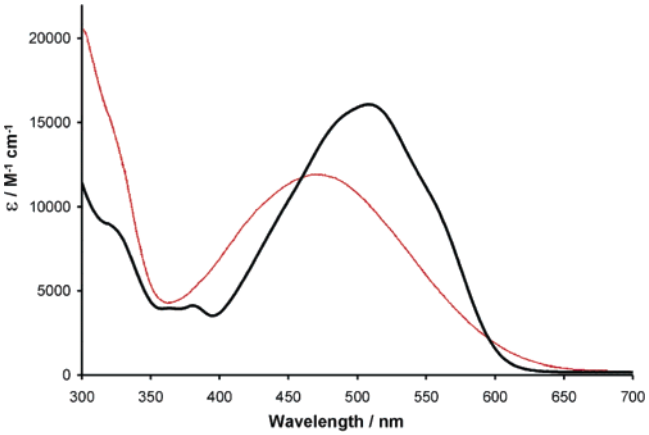

Figure 4. Electronic absorption spectra of $[(^tBuCO_2)_3Mo_2]_2[\mu\text{-}C_6H_2\text{-}2,5\text{-}(OH)_2\text{-}1,4\text{-}(CO_2)_2]$ (black) and of $[(^tBuCO_2)_3Mo_2]_2[\mu\text{-}O_2C{-}C_6F_4{-}CO_2]$ (red).

cm^{-1}, although as shown in Figure 2, for the C_6F_4 and C_6H_4 bridge-containing compounds, these are dwarfed by the lower energy metal-to-bridge charge transfer. The absorptions in the 300 to 400 nm range arise from M_2 δ-to-CO_2 π^* transitions associated with the pivalate groups, and they are present in the parent compounds $M_2(O_2C^tBu)_4$ (M = Mo, W).

The spectra of $[(^tBuCO_2)_3M_2]_2[\mu\text{-}O_2C{-}Ar{-}CO_2]$ compounds [Ar = C_6H_4, C_6F_4, C_6Cl_4, C_6H_2-2,5-$(OH)_2$] recorded as Nujol mulls are given in the Supporting Information and are quite different from those observed in solution. This difference arises from the association of one M_4 unit with its neighbors by way of $M\cdots O_{carboxylate}$ electrostatic interactions that result in a ladderlike structure in the solid state.[10,12] As observed for $[(^tBuCO_2)_3M_2]_2[\mu\text{-}O_2C{-}C_6F_4{-}CO_2]$, it is likely that the phenyl ring twists in order to accommodate these $M\cdots O_{carboxylate}$ interactions, resulting in larger values for θ_1 and θ_2, shifting λ_{max} to higher energy. In this regard, the electronic absorption spectra are very similar to those of large aromatic molecules which have very distinctive spectral features when present as a monomer relative to when they associate due to $\pi\cdots\pi$ stacking.

The electronic spectra of the compounds in which the phenyl ring is substituted in the 2 and 5 positions by hydroxyl groups are also worthy of particular attention. The solution electronic absorption spectrum for the molybdenum complex is shown in Figure 4 where it is compared with the perfluoroterephthalate analogue. The band shape and its position imply that the planar conformation of the dihydroxy-substituted molecule is favored at room temperature as might be expected if intramolecular hydrogen bonding is occurring and as predicted by the gas-phase calculations on the model compounds $[(HCO_2)_3M_2]_2[\mu\text{-}C_6H_2\text{-}2,5\text{-}(OH)_2\text{-}1,4\text{-}(CO_2)_2]$.

As a further test of the effect of hydrogen bonding, $[(^tBuCO_2)_3Mo_2]_2[\mu\text{-}C_6H_2\text{-}2,5\text{-}(OH)_2\text{-}1,4\text{-}(CO_2)_2]$ has been treated in THF with 2 equiv of Bu_4NOH from a 1 M MeOH solution, resulting in bleaching of the intensely colored solution from red to yellow. We propose that deprotonation of the phenolic protons occurs and that phenolate anion O^--to-carboxylate oxygen electrostatic repulsion leads to twisting of the aromatic ring, thus removing M_2 δ-to-C_6 π-conjugation. This is displayed in eq 2, although we cannot be sure of the exact mode of bonding in the "off" position. Treatment with an $H^+BF_4^-/Et_2O$

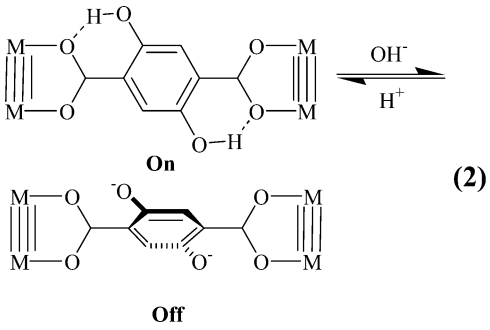

(2)

solution restores the original color, completing the switching cycle, as evidenced by the electronic absorption spectra shown in Figure 5.

Radical Cations. Oxidation of the neutral bridged complexes with $Ag^+PF_6^-$ in THF generates the oxidized radical cations which, though chemically labile, do persist long enough for reasonable characterization in solution. Broadly speaking, the Mo_4-containing cations can be classified as Class II, and the W_4-containing cations, as Class III based on analysis of their IVCT (Class II system) or charge resonance (Class III system) bands in the NIR region of the electronic absorption spectrum.[4] The NIR spectra of the related molybdenum and tungsten cations for the C_6H_2-2,5-$(OH)_2$ bridge are compared in Figure 6. The time-dependent decay of the spectrum of the W_4-containing perfluoroterephthalate-bridged radical cation is shown in Figure 7.

The common feature for the W_4-containing symmetrically bridged radical cations is the appearance of a low energy, infrared absorption. The relatively narrow and intense absorption is characteristic of a charge resonance band associated with a Class III, delocalized mixed-valence compound.[20] The spectroscopic parameters associated with these absorptions are listed in Table 3. For each W_4-containing compound, the bandwidth is narrower than that predicted by the Hush model[21,22] for a Class II compound. As can be seen from an inspection of the data in Table 3, the magnitude of H_{ab} tracks directly with the calculated HOMO−LUMO energy gap (Tables 1 and 2), which in turn correlates with the splitting of the two M_2 δ combinations. Potential energy curves comparing $[(^tBuCO_2)_3Mo_2]_2[\mu\text{-}C_6H_2\text{-}2,5\text{-}(OH)_2\text{-}1,4\text{-}(CO_2)_2]$ (Class II) with $[(^tBuCO_2)_3W_2]_2[\mu\text{-}C_6H_2\text{-}2,5\text{-}(OH)_2\text{-}1,4\text{-}(CO_2)_2]$ (Class III) are given in Figure 8. It is also interesting to see for Class III compounds that as H_{ab} gets smaller, the shape of the low-energy IVCT band gets more asymmetric and becomes broader. This is as predicted for a two-state model where the ground-state potential well becomes increasingly shallow as it approaches the Class II/III border. Conversely, as H_{ab} increases, the band shape gets narrower and more gaussian. This is because the electronic transition becomes more molecular and represents taking an electron from a bonding MO and placing it in a nonbonding or weakly antibonding one. Due to the intensity and sharpness of the IVCT absorption for $[(^tBuCO_2)_3W_2]_2[\mu\text{-}O_2CC_6H_4CO_2]$, we have tentatively assigned this compound as Class III. However, the calculated and experimentally observed $\Delta\bar{\nu}_{1/2}$ values are close in energy, and the fact that only a small K_c value is observed electrochemically,

(20) (a) Creutz, C. *Prog. Inorg. Chem.* **1983**, *30*, 1. (b) Crutchley, R. J. *Adv. Inorg. Chem.* **1994**, *41*, 273.
(21) Hush, N. S. *Coord. Chem. Rev.* **1985**, *64*, 135.
(22) Hush, N. S. *Prog. Inorg. Chem.* **1967**, *8*, 391.

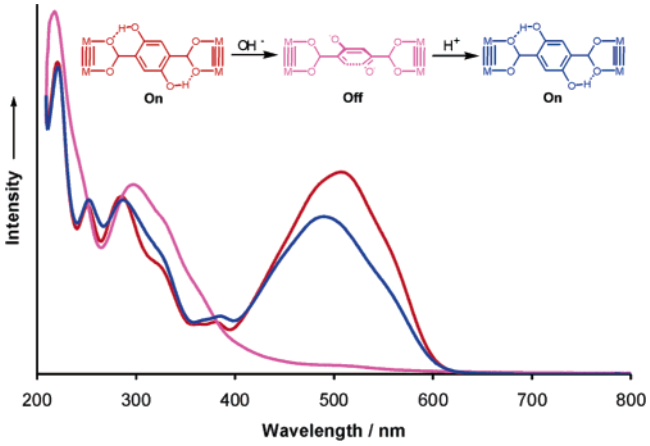

Figure 5. Chemical "switching" of $[(^tBuCO_2)_3Mo_2]_2[\mu\text{-}C_6H_2\text{-}2,5\text{-}(OH)_2\text{-}1,4\text{-}(CO_2)_2]$ in THF at room temperature along with proposed structures as the carriers of those spectral signatures.

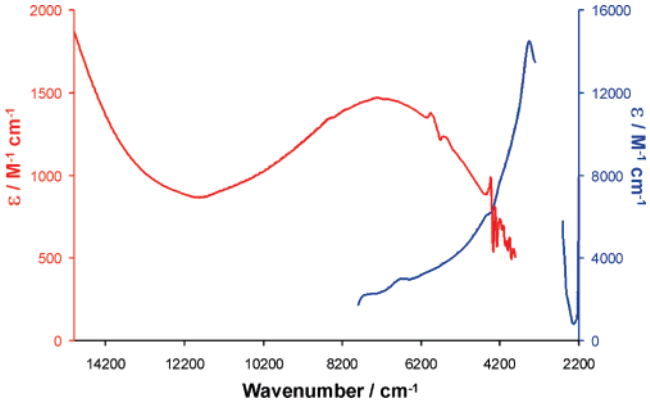

Figure 6. NIR electronic absorption spectra of $[(^tBuCO_2)_3M_2]_2[\mu\text{-}C_6H_2\text{-}2,5\text{-}(OH)_2\text{-}1,4\text{-}(CO_2)_2]^+PF_6^-$ [M = Mo (red) and W (blue)] in THF at room temperature. The gap between 2610 and 3280 cm^{-1} for $[(^tBuCO_2)_3W_2]_2[\mu\text{-}C_6H_2\text{-}2,5\text{-}(OH)_2\text{-}1,4\text{-}(CO_2)_2]^+PF_6^-$ corresponds to a THF solvent absorption.

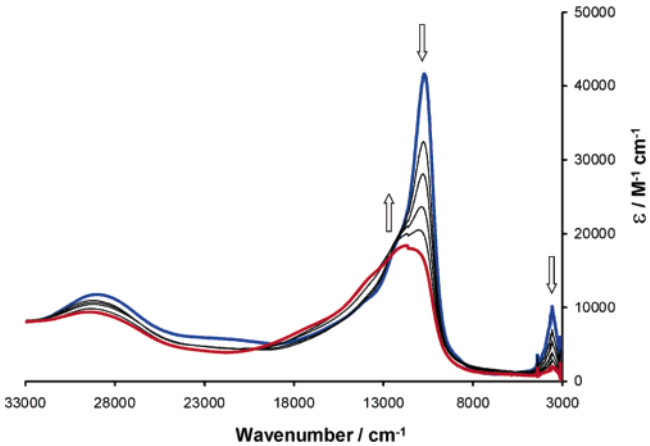

Figure 7. Time dependent decay of $[(^tBuCO_2)_3W_2]_2[\mu\text{-}O_2C\text{-}C_6F_4\text{-}CO_2]^+PF_6^-$ in THF at room temperature, with spectra acquired at time intervals between t = 3 min (blue) and t = 420 min (red).

vide infra, may indicate that this compound is close to the Class II/III borderline.

For these W_4-containing radical cations, we also observe an intense ($\epsilon \approx 50\,000$ M^{-1} cm^{-1}) higher-energy absorption assignable to the SOMO-to-LUMO transition. This is the ML(bridge)CT absorption, and it occurs at slightly lower energy than the related transition in the neutral complexes. It is sharper, is not significantly temperature-dependent, and does not have the vibronic features exhibited by the neutral complexes. At higher energy still (300−400 nm), we also observe a less-intense MLCT band involving the CO_2 π * orbitals of the pivalate ligands. This is moved to slightly higher energy in relation to the related band of the neutral complexes consistent with a stabilization of the M_2 δ manifold as a result of the increase in charge on the metal atoms.

In contrast, the spectrum of the Mo_4-containing radical cation shown in Figure 6 is decidedly differently. The broad Gaussian shaped absorption in the near-IR centered at λ = 1390 nm corresponds to the E_{op} of a Class II mixed-valence compound (see Figure 8).

The radical cations of the bridged 2,6-dichloro- and tetrachloroterephthalate-bridged compounds were notably less stable and did not allow for a quantitative study, but it is fair to state that these cations are not delocalized and the W_2 centers are only weakly coupled as a result of the CO_2/C_6 dihedral angle being twisted from planar in the ground-state geometry.

Electrochemical Measurements. The compounds studied showed two oxidation waves by cyclic voltammetry (CV) and differential pulse voltammetry (DPV). The first oxidation is reversible on the CV time scale, while the second is quasi-reversible. The tungsten compounds are easier to oxidize relative to the molybdenum compounds, and the separation between the first and second oxidation waves, $\Delta E_{1/2}$, is also greater for tungsten, as is shown in Figure 9 for the pair of compounds having the 2,5-dihydroxy-substituted aryl ring. The magnitude of $\Delta E_{1/2}$ provides a direct measure of the relative stability of the monocation in relation to the neutral and doubly oxidized species, as shown in eq 3 below.[23] The K_c value, the equilibrium constant involving the formation of the monocation, is commonly employed as an indicator of the degree of electronic coupling. The electrochemical data for the various compounds under study in this work are listed in Table 4.

$$[M_2{-}O_2C{-}Ar{-}CO_2{-}M_2] + [M_2{-}O_2C{-}Ar{-}CO_2{-}M_2]^{2+} \overset{K_c}{\rightleftharpoons} 2\,[M_2{-}O_2C{-}Ar{-}CO_2{-}M_2]^{+} \quad (3)$$

$$K_c = e^{\Delta E_{1/2}/25.69}$$

It is immediately apparent that K_c is larger for tungsten than for molybdenum. However, the relative magnitudes of K_c for the tungsten complexes are quite modest with respect to those of the Creutz−Taube ion and related oxalate-bridged species of these metals: for oxalate-bridge cations, $K_c = \sim 10^{12}$ (M = W) and $\sim 10^4$ (M = Mo) and for $[(NH_3)_5Ru(pz)Ru(NH_3)_5]^{5+}$, $K_c = \sim 10^6$. As noted elsewhere,[24] great care should be taken in the interpretation of electrochemical data and its correlation with Class III or Class II behavior, as K_c may vary with solvent and electrolyte counterions. In addition, as the number of redox-active centers increases, the value of K_c is expected to decrease, and Class III behavior may be observed at relatively small K_c values. It is also important to remember that the electrochemical data do not, by themselves, inform one of what is being oxidized

(23) Richardson, D. E.; Taube, H. *Inorg. Chem.* **1981**, *20*, 1278.
(24) (a) D'Alessandro, D. M.; Keene, F. R. *Dalton Trans.* **2004**, 3950. (b) Barriere, F.; Camire, N.; Geiger, W. E.; Mueller-Westerhoff, U. T.; Sanders, R. *J. Am. Chem. Soc.* **2002**, *124*, 7262. (c) Chisholm, M. H.; Clark, R. J. H.; Gallucci, J. C.; Hadad, C. M.; Patmore, N. J. *J. Am. Chem. Soc.* **2004**, *126*, 8303.

Table 3. Summary of the Experimental Parameters of the IVCT Bands Observed in the Electronic Absorption Spectra of $[(^tBuCO_2)_3M_2]_2[\mu\text{-}O_2C{-}Ar{-}CO_2]^+PF_6^-$ (M = Mo, W) Radical Cations[a]

Ar	$\bar{\nu}_{max}$/ cm^{-1}	$\Delta\bar{\nu}_{1/2}$(observed)[b]/ cm^{-1}	$\Delta\bar{\nu}_{1/2}$(calculated)[c]/ cm^{-1}	ϵ_{max}/ M^{-1} cm^{-1}	H_{ab}[d]/ cm^{-1}
		M = W			
C_6H_4	3220	2220	2727	18 000	1610
C_6F_4	3570	582	2872	9600	1785
C_6Cl_4[e]					
$C_6H_2{-}2,5\text{-}Cl_2$	3391	840	2799	10 300	1696
$C_6H_2{-}2,5\text{-}(OH)_2$	3430	1270	2815	14 400	1715
$C_6H_5{-}2\text{-}F$	3453	1461	2824	14 000	1726
$C_6H_2{-}2,6\text{-}Cl_2$[e]					
		M = Mo			
$C_6H_2{-}2,5\text{-}(OH)_2$[f]	7200	5720	4078	1470	446

[a] Spectra were acquired at 298 K in THF solvent. [b] For nonsymmetrical absorptions, $\Delta\bar{\nu}_{1/2}$ was determined from analysis of the band on the high energy side of $\bar{\nu}_{max}$ to avoid low energy cutoff effects. [c] Calculated using $\Delta\bar{\nu}_{1/2} = [2310\bar{\nu}_{max}]^{1/2}$ (at room temperature).[2] [d] For Class III systems [$\Delta\bar{\nu}_{1/2}$(calcd) $\gg$ $\Delta\bar{\nu}_{1/2}$(obsd)], $H_{ab} = \bar{\nu}_{max}/2$. [e] Radical cation was too unstable to obtain data. [f] Class II system, hence according to the Hush model,[21] $H_{ab} = [(4.2 \times 10^{-4})\epsilon\Delta\bar{\nu}_{1/2}\bar{\nu}_{max}]^{1/2}/d$, with d (11.3 Å) approximated using the optimized geometry from the gas-phase DFT calculations.

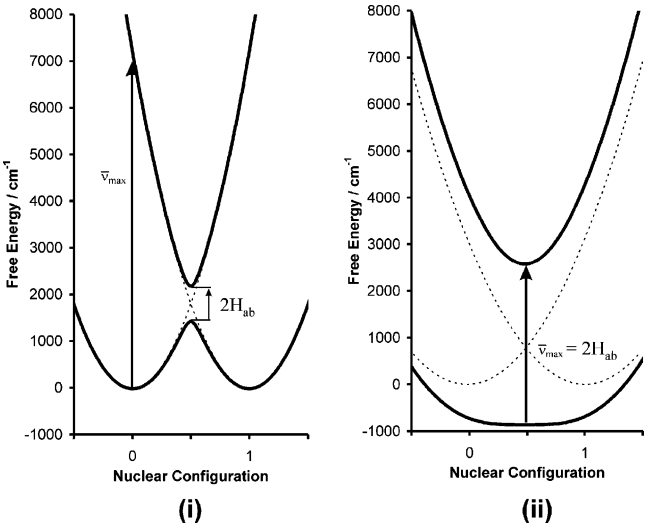

Figure 8. Potential energy curves for Class II (i) and Class III (ii) systems. Values for $\bar{\nu}_{max}$ and H_{ab} were obtained from the experimental data for $[(^t\text{-}BuCO_2)_3Mo_2]_2[\mu\text{-}C_6H_2\text{-}2,5\text{-}(OH)_2\text{-}1,4\text{-}(CO_2)_2]^+$ (i) and $[(^tBuCO_2)_3W_2]_2[\mu\text{-}C_6H_2\text{-}2,5\text{-}(OH)_2\text{-}1,4\text{-}(CO_2)_2]^+$ (ii). See Table 3. The dotted lines represent the corresponding diabatic (Class I) curves.

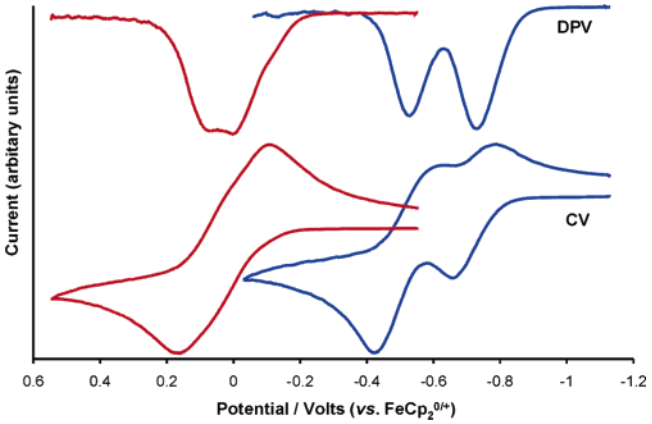

Figure 9. Cyclic voltammogram (CV) and differential pulse voltammogram (DPV) for $[(^tBuCO_2)_3M_2]_2[\mu\text{-}C_6H_2\text{-}2,5\text{-}(OH)_2\text{-}1,4\text{-}(CO_2)_2]$ [M = Mo (red) and W (blue)] in a 0.1 M $^nBu_4NPF_6$/THF solution.

(or reduced). This could be metal- or bridge-based and in succession or in combination. Despite these cautionary notes, careful comparison of K_c values for similar compounds under identical experimental conditions can be useful. We note here,

Table 4. Summary of Electrochemical Data for $[(^tBuCO_2)_3M_2]_2[\mu\text{-}O_2C{-}Ar{-}CO_2]$ (M = Mo, W) Compounds[a]

compound (X)	$E_{1/2}(1)$/V	$E_{1/2}(2)$/V	$\Delta E_{1/2}$/mV	K_c
		M = W		
C_6H_4	−0.34	−0.18	160	5.1×10^2
C_6F_4	−0.66	−0.37	285	6.6×10^4
C_6Cl_4[b]	−0.11			
$C_6H_2{-}2,5\text{-}Cl_2$	−0.72	−0.44	274	4.3×10^4
$C_6H_2{-}2,5\text{-}(OH)_2$	−0.72	−0.52	202	2.6×10^3
$C_6H_5{-}2\text{-}F$	−0.76	−0.54	220	5.2×10^3
$C_6H_2{-}2,6\text{-}Cl_2$	−0.60	−0.39	216	4.5×10^3
		M = Mo		
C_6F_4[c]	0.10		65	1.3×10^1
$C_6H_2{-}2,5\text{-}(OH)_2$	0.00	0.08	79	2.1×10^1

[a] Voltammograms were recorded in a 0.1 M NBu_4PF_6/THF solution and referenced to the $FeCp_2^{0/+}$ couple by addition of a small amount of ferrocene to the sample. [b] One two-electron process observed. [c] Values obtained from ref 13.

for example, that the magnitude of K_c for the complexes in Table 4 roughly tracks with the HOMO−LUMO energy gap (Table 1) and the magnitude of H_{ab} (Table 3).

EPR Spectroscopic Studies. The EPR spectra of radical cations recorded in THF reliably establish that the metal centers are being oxidized. The g values are well reduced from the spin-only value as a result of spin−orbit coupling, and this is greater for the 5d metal W relative to Mo. In addition, the central signal is flanked by a satellite spectrum due to coupling to the spin-active nuclei of each metal [$^{95/97}$Mo or ^{183}W]. From these data, one may reliably determine whether the single electron is valenced-trapped on one M_2^{5+} center in a δ orbital or is delocalized over all four metal atoms, and this is a matter we have discussed before.[6,25] When classifying localized or delocalized behavior, the time scale of the experiment used is important, and delocalization on the EPR time scale, $\sim 10^{-9}$ s, is, of course, slower than that determined from electronic spectroscopy, $\sim 10^{-15}$ s.

The EPR spectrum of $[(^tBuCO_2)_3Mo_2]_2[\mu\text{-}C_6H_2\text{-}2,5\text{-}(OH)_2\text{-}1,4\text{-}(CO_2)_2]^+$ is given in Figure 10. The signal has $g_{iso} = 1.942$ and $A_{iso} = 27.2$ G, which are very close in value to those recently reported for $Mo_2(O_2C^tBu)_4^+$.[25] This demonstrates that the single electron is localized on just one Mo_2^{5+} unit. In contrast, the EPR spectrum of $[(^tBuCO_2)_3W_2]_2[\mu\text{-}C_6H_2\text{-}2,5\text{-}(OH)_2\text{-}1,4\text{-}(CO_2)_2]^+$, shown in Figure 11, has a main signal at

(25) Chisholm, M. H.; D'Acchioli, J. S.; Pate, B. D.; Patmore, N. J.; Dalal, N. S.; Zipse, D. J. *Inorg. Chem.* **2005**, *44*, 1061.

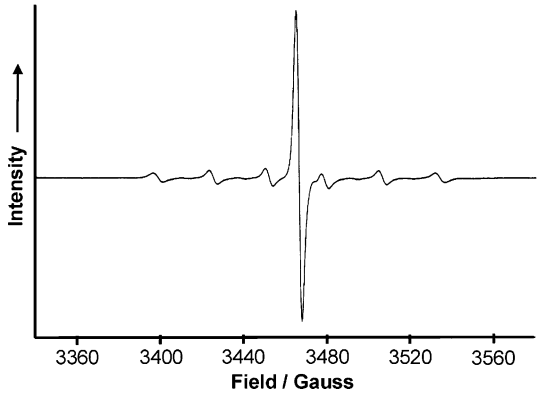

Figure 10. EPR spectrum of $[(^t BuCO_2)_3Mo_2]_2[\mu\text{-}C_6H_2\text{-}2,5\text{-}(OH)_2\text{-}1,4\text{-}(CO_2)_2]^+PF_6^-$ in THF at 210 K.

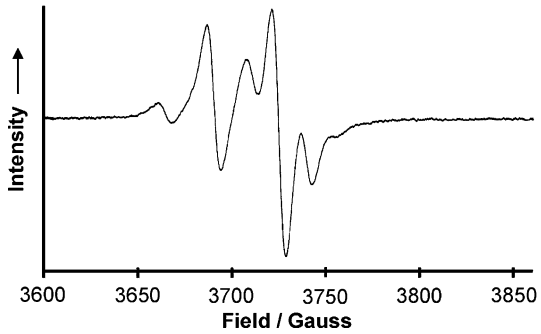

Figure 11. EPR spectrum of $[(^t BuCO_2)_3W_2]_2[\mu\text{-}C_6H_2\text{-}2,5\text{-}(OH)_2\text{-}1,4\text{-}(CO_2)_2]^+PF_6^-$ in THF at 210 K.

$g_{iso} = 1.805$ (3725 G), and a second species of lower concentration to lower field. The hyperfine coupling $A_{iso} = 29.3$ G and intensity distribution of the hyperfine spectrum indicates that the main species has a single electron delocalized over four tungsten atoms and is assigned to the $[(^t BuCO_2)_3W_2]_2[\mu\text{-}C_6H_2\text{-}2,5\text{-}(OH)_2\text{-}1,4\text{-}(CO_2)_2]^+$ radical cation. The impurity to lower field grows in concentration relative to $[(^t BuCO_2)_3W_2]_2[\mu\text{-}C_6H_2\text{-}2,5\text{-}(OH)_2\text{-}1,4\text{-}(CO_2)_2]^+$ over a period of hours at room temperature and is assigned to the $W_2(O_2CBu^t)_4^+$ ion, formed by ligand redistribution reactions. The lack of other EPR-active species is noteworthy and may well indicate that redox disproportionation reactions of the type

$$2M_2^{5+} \rightleftharpoons M_2^{4+} + M_2^{6+}$$

are also occurring. M_2^{6+} and M_2^{4+} species would be diamagnetic with triple and quadruple bonds, respectively, as seen for $W_2(O_2C^tBu)_6$ and $W_2(O_2C^tBu)_4$.[19,26] Similar behavior is observed for $[(^t BuCO_2)_3W_2]_2[\mu\text{-}O_2C\text{-}C_6H_4\text{-}CO_2]^+$, which has $g_{iso} = 1.806$ and $A_{iso} = 28.4$ G.

Concluding Remarks

The series of compounds studied in this work reveal most clearly how the electronic coupling of two dinuclear centers is determined by electronic factors associated with the metal centers and the central bridge. For the general representation of a symmetrical system as $[M_2]O_2C\text{-}X\text{-}CO_2[M_2]$, there are two key parameters determining the degree to which the two M_2 centers are coupled.[27]

The first we can term α which, as shown in **V**, relates to the $[M_2]\text{-}O_2C$ coupling. In our study, since CO_2 is invariant, the attenuation of the α parameter is determined by $[M_2]$, and for a given ligand set, (i.e., pivalate), the sole influence on α is M = Mo vs W. Thus, the greater electronic coupling seen for the

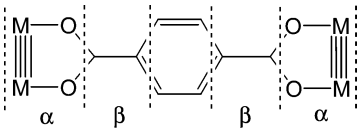

V

W_4-containing complexes is a result of the greater W_2 δ orbital interaction with the CO_2 π (and π*) system. As has been shown, this typically leads to fully delocalized, Class III behavior for tungsten in relation to valence-trapped Class II behavior for molybdenum in their radical cations. For the W_4-containing cations, the odd electron is fully delocalized over four tungsten atoms separated by 11 Å by the aryldicarboxylate bridge. This α term can be modified by changing CO_2 to COS and CS_2, and we shall show the effect of these perturbations in a future work.

The second term, β, represents the degree of coupling that exists between the CO_2 π-system and the π-system of the C_6 ring. This, of course, is independent of CO_2 but can be modified both by the orbital energies of the C_6 π system and by the O_2C-C_6 ring dihedral angle. This work has nicely demonstrated the influence of both of these factors within the series C_6X_4 where X = H, F, and Cl and for $C_6H_2X_2$ where X = Cl or OH. The preferred orientation of the angles θ_1 and θ_2 can be independently controlled by steric interactions, hydrogen bonding, or temperature. The rotational barriers involving the O_2C-C_6 moiety, together with the HOMO−LUMO energy gap, control the thermochromic effects observed in this series of compounds. Hence, the aromatic spacer acts as a molecular rheostat between two M_2 units with the coupling being controlled by functionalization and temperature. We have also suggested that the O_2C-C_6 ring dihedral angles can be controlled chemically as in the deprotonation of the 2,5-dihydroxyterephthalate-bridged complexes, thereby providing a chemical switch between "on and off" coupled M_2 centers. In the chemistry described herein, this reaction is not fully reversible, but it does indicate the potential for the design of a molecular sensor or switch based upon chemically labile groups in the 2,5-position of terephthalate linkers.

One final point worthy of emphasis is that the electronic coupling in the radical cations occurs exclusively as a result of mediation via the π* system of the bridge. In the super-exchange mechanism, this correlates with electron hopping/transfer. The HOMO of the bridge π-system does not participate in a hole-hopping transfer, and no L(bridge)MCT band is observed in the electronic spectra of the radical cations; none is predicted to have any significant oscillator strength from the TD-DFT calculations. The filled carboxylate π MOs are too low in energy to interact significantly with the M_2 δ or δ* orbitals.

Acknowledgment. The National Science Foundation is thanked for funding, and the Ohio Supercomputer Center is gratefully acknowledged for generous allocation of computing

(26) Chisholm, M. H.; Heppert, J. A.; Hoffman, D. M.; Huffman, J. C. *Inorg. Chem.* **1985**, *24*, 3214.
(27) Launay, J.-P. *Chem. Soc. Rev.* **2001**, *30*, 386.

time. Dr. Kari Green-Church is thanked for assistance in obtaining the MALDI-MS data.

Supporting Information Available: Details of the synthesis and characterization of the newly prepared compounds, together with the solid-state electronic absorption spectra for selected $[(^tBuCO_2)_3M_2]_2[\mu\text{-}O_2CArCO_2]$ compounds. Calculated coordinates for the preferred ground state conformers of $[(HCO_2)_3M_2]_2[\mu\text{-}O_2CArCO_2]$ compounds and full citations from main ms. This material is available free of charge via the Internet at http://pubs.acs.org.

JA0550982